Fine Chemical Engineering
https://ojs.wiserpub.com/index.php/FCE/

Research Article

Adsorption of Methyl Red Using Agricultural Waste-Derived Adsorbents: A Case Study with Argan Nut Shells

Mohamed Sadoq[1], Mbarka Ouchabi[2], Abderahim Kali[1], Hafssa Atlas[1], Nicolas Joly[3], Patrick Martin[3], Hassan Lgaz[4], Alexis Spalletta[3], Fatima Boukhlifi[1*]

[1]Laboratory of Chemistry and Biology Applied to the Environment, URL-CNRST No. 13, Faculty of Sciences, Moulay Ismail University, Meknes, 50050, Morocco
[2]Laboratory of Catalysis and Corrosion of Materials, Faculty of Sciences, Chouaïb Doukkali University, El Jadida, 24000, Morocco
[3]Unit Transformations & Agroressources (ULR7519), University of Artois, 62408 Béthune, France
[4]Innovative Durable Building and Infrastructure Research Center, Center for Creative Convergence Education, Hanyang University ERICA Campus, 55 Hanyangdaehak-ro, Sangrok-gu, Ansan-si, 15588, Gyeonggi-do, Republic of Korea
E-mail: f.boukhlifi@umi.ac.ma

Received: 29 July 2025; **Revised:** 10 October 2025; **Accepted:** 13 October 2025

Graphical Abstract:

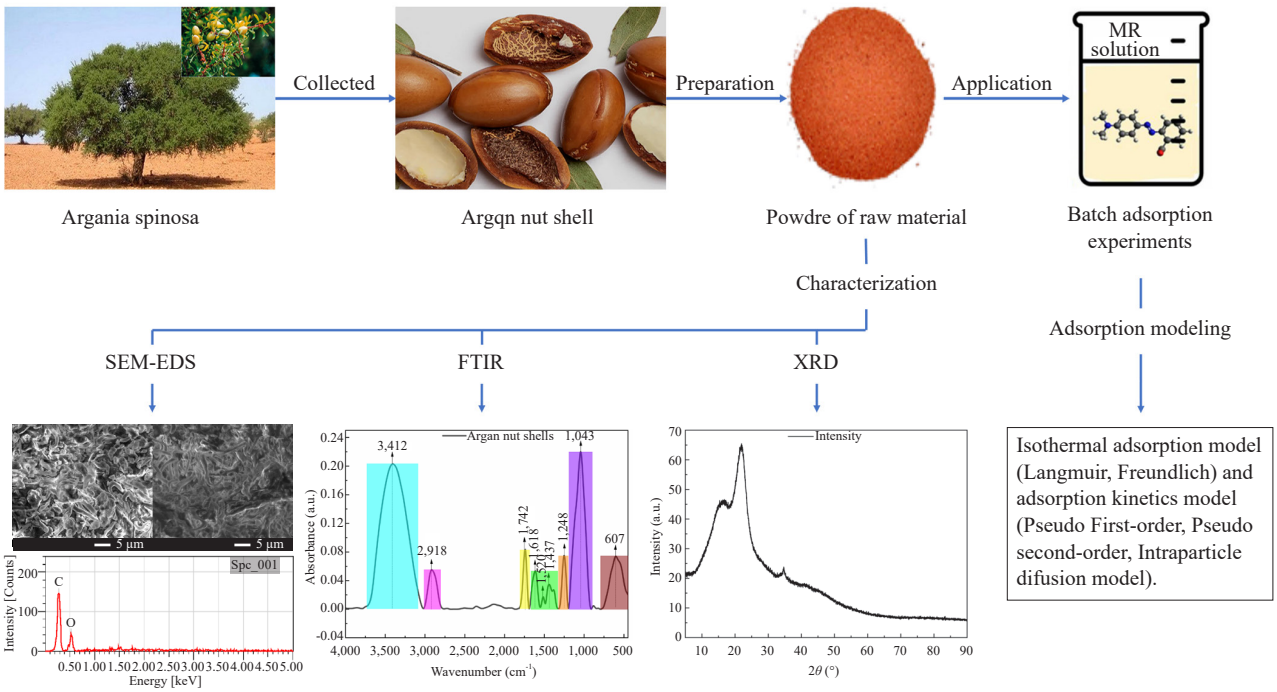

Abstract: The effluents from textile and tannery industries contain high levels of synthetic dyes such as Methyl Red (MR), which represent a serious threat to aquatic ecosystems and human health due to their toxicity and persistence.

Copyright ©2025 Fatima Boukhlifi, et al.
DOI: https://doi.org/10.37256/fce.7120268045
This is an open-access article distributed under a CC BY license
(Creative Commons Attribution 4.0 International License)
https://creativecommons.org/licenses/by/4.0/

To search for cost-effective and sustainable adsorbents derived from agricultural residues is therefore an urgent environmental priority. In this study, Argan Nut Shells (ANS), an abundant byproduct of argan oil production, were investigated as a low-cost adsorbent for MR removal. Adsorption performance was evaluated under different conditions, and results showed that 80 mg of ANS removed 53.5% of MR from 20 mL of solution. Although this efficiency appears modest, it remains competitive when compared with other natural adsorbents such as rice husk and coconut shells, particularly considering the economic and ecological value of valorizing argan residues. Kinetic modeling demonstrated that the adsorption process followed a pseudo-second-order model, with intraparticle diffusion not being the sole rate-limiting step, while equilibrium was reached after 80 minutes of contact. The Freundlich model, indicating a heterogeneous adsorption surface, best described the adsorption isotherms. Thermodynamic parameters revealed that the adsorption of methyl red onto ANS was spontaneous ($\Delta G° < 0$) and exothermic ($\Delta H° < 0$). The point of zero charge (pH_{PZC}) value was determined to be 3.68. Fourier-Transform Infrared Spectroscopy (FTIR), X-Ray Diffraction (XRD), Scanning Electron Microscopy (SEM), and Energy-Dispersive X-Ray Spectroscopy (EDS) analyses confirmed surface modification after MR adsorption and provided insights into the interaction mechanism.

***Keywords*:** adsorption, argan nut shells, methyl red, kinetic, Freundlich

1. Introduction

In recent years, significant attention has been focused on the environmental impact of pollutants stemming from textile dyeing due to their detrimental effects on aquatic ecosystems.[1,2] These effects include reducing light penetration, disrupting photosynthesis in aquatic plants, and causing oxygen depletion, which can destabilize ecosystems and harm aquatic organisms. Among these pollutants, Methyl Red (MR),[3,4] a synthetic dye widely used in various industries,[5,6] poses a significant threat due to its persistent nature and potential toxicity.[7] Consequently, efforts to mitigate its presence and reduce environmental contamination have led to the exploration of sustainable and effective remediation methods such as advanced oxidation,[8] electro-degradation,[9] catalysis[10] and adsorption[11-13]. This last solution represents a promising approach, especially considering the use of natural adsorbents such as raw chitin,[14] clays,[15,16] activated carbon,[17-19] zeolites,[20,21] and Argan Nut Shells (ANS).[22,23]

ANS represents an underutilized co-product of argan oil production, abundantly available in argan-producing regions. They provide an economical and sustainable alternative due to their low cost, wide accessibility, and inherent adsorption capabilities. The valorization of this agricultural by-product not only tackles waste management challenges but also contributes to the development of eco-friendly and efficient solutions for pollutant removal.[24]

The adsorption process involves the adherence of molecules or particles onto the surface of a solid material, making it an attractive method for removing contaminants from aqueous solutions.[25] In this context, the adsorption of MR onto ANS emerges as a focal point for investigation due to its potential as an eco-friendly and efficient remediation approach.

This study aims to elucidate the parameters governing the adsorption process, specifically kinetics, isotherms, thermodynamics, and surface characterization. Understanding these aspects is crucial for optimizing the adsorption efficiency and unveiling the fundamental interactions between MR molecules and the surface of argan nut shells.

Firstly, the investigation focuses on a meticulous examination of the adsorption kinetics, aiming to ascertain the rate and mechanism of MR uptake onto ANS. Subsequently, isotherm studies will elucidate the equilibrium adsorption capacity and behavior of MR at varying concentrations. Moreover, thermodynamic analysis will provide insights into the spontaneity, heat change, and stability of the adsorption process.

Furthermore, this study includes a detailed characterization of the argan nut shell surface before and after MR adsorption using Fourier-Transform Infrared Spectroscopy (FTIR) and X-Ray Diffraction (XRD). Scanning Electron Microscopy (SEM) and Energy-Dispersive X-Ray Spectroscopy (EDS) techniques will be employed only before adsorption to analyze the structure and chemical composition of the ANS.

2. Materials and methods

2.1 *Chemicals*

All the chemicals used in this study were of analytical grade. Figure 1 depicts the chemical structure of methyl red, with a molecular formula of $C_{15}H_{15}N_3O_2$. Sodium hydroxide (NaOH, 98%), hydrochloric acid (HCl, 37%), and sodium chloride (NaCl, 99.8%) compounds were supplied by Sigma-Aldrich and used without further purification. All stock solutions were prepared with distilled water from POBEL for the preparation of materials and adsorption tests.

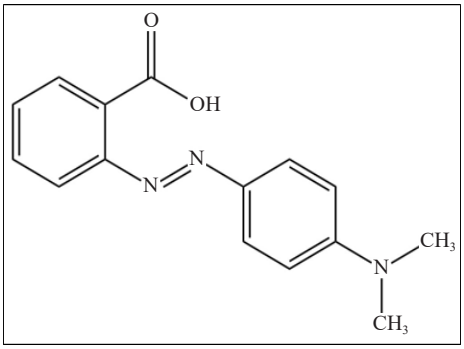

Figure 1. Chemical structure of methyl red

2.2 *Preparation of argan nut shells*

ANS were collected from a cooperative in the Agadir region, Morocco. After washing with distilled water and drying at 100 °C for 24 h, the shells were ground and sieved to obtain particles smaller than 100 µm. This size range was selected to maximize surface area and enhance adsorption efficiency. The prepared ANS were stored in airtight containers until use (Figure 2).

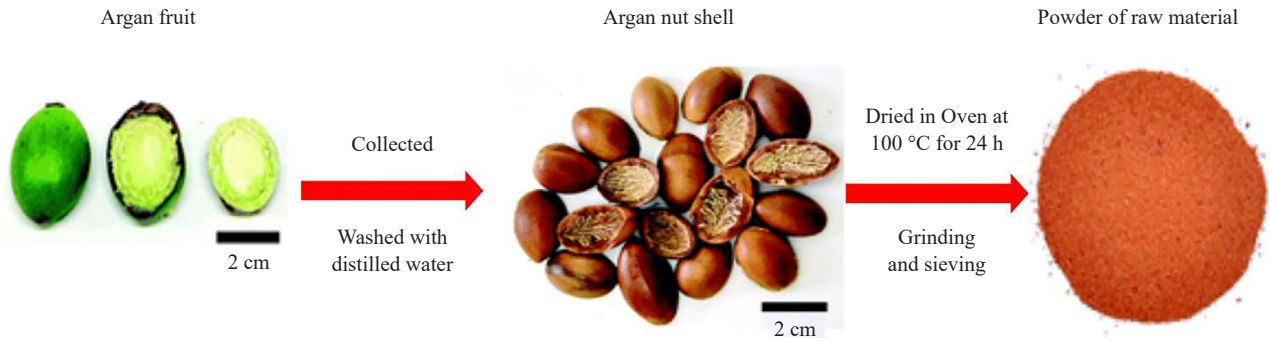

Figure 2. Preparation of argan nut shells

2.3 *Characterization of adsorbent*

FTIR spectroscopy, conducted using a Shimadzu FT-IR IRAffinity-1S, was used to analyze the molecular structure of the adsorbent before and after MR adsorption. XRD analysis was carried out using a Bruker D8 ADVANCE diffractometer with Cu Kα radiation (λ = 1.5406 Å) to investigate the crystallinity of the material. Diffraction patterns were recorded over a 2θ range of 2°–90° with a step size of 0.02° and a scanning rate of 1°/min, ensuring high precision

in peak position, intensity, and resolution. The surface morphology was studied using a JEOL JSM-IT500HR SEM, which provides high-resolution imaging with its high-brightness electron gun system, enabling rapid analysis with high sensitivity and spatial resolution. Elemental analysis was carried out using an EDS system and determination of the pH_{PZC} to assess its zero-surface charge.

FTIR plays a crucial role in the identification of surface chemical groups. The sample is composed of 5% solid material and 95% KBr, meticulously ground and pressed using a pellet press to create a compact pellet. This pellet is subsequently positioned along the path of the infrared beam. KBr facilitates the exclusive recording of absorption bands originating from the analyzed solid. Spectra, acquired with a resolution of 4 cm^{-1}, necessitate 64 scans.

The X-ray diffraction technique involves irradiating a solid sample with radiation of wavelengths ranging between 0.1 and 10 nanometers, at various 2θ angles. When the radiation diffracted by the atomic planes of the solid is in phase, it generates a coherent beam that is then detected. To characterize these samples, the diffractograms, recorded between 2θ angles of 0° to 90°, allow for the analysis of the crystalline structure and identification of different phases present within the material.

The SEM used not only allows for the observation of the surface morphology of our adsorbent but also the determination of its chemical composition through an EDS associated with SEM. The principle involves bombarding the surface of the solid, previously coated with carbon or gold to make it conductive, with an electron beam. The atoms in the sample release electrons that are processed by a detector, providing an image of the sample's surface.

To determine the point of zero charge (pH_{PZC}), the solid addition method was employed.[26] 50 mL of a 0.01 M NaCl solution was poured into several beakers, and then the initial pH was adjusted using HCl or NaOH solutions within a range of 2 to 12. Precisely 1 g of the adsorbent was then added to each beaker, and the samples were kept in agitation, in contact with the solution, for 24 h. At the end of this period, the final pH of the solutions was measured. The determination of the pH_{PZC} was achieved by identifying the point of intersection on the curve representing the change in final pH relative to the initial pH (pH_f-pH_i as a function of pH_i). This method allowed us to establish the pH_{PZC} with precision.

2.4 *Adsorption experiment*

The adsorption experiments were carried out in a controlled environment to assess the effectiveness of argan nut shells. For each experiment, a specific quantity of shells was added to a flask containing 20 mL of methyl red at an initial concentration of 30 mg/L. Subsequently, the mixture was placed in a temperature-controlled bath to maintain a stable temperature, thus ensuring uniform conditions throughout the experiment. The pH was adjusted to between 2 and 12 using HCl or NaOH solutions to evaluate adsorption under acidic, natural, and alkaline conditions.

After each contact time, the mixture underwent centrifugation at 2,500 revolutions per minute to separate the solid phase from the solution. The liquid phase was then subjected to filtration using a microporous filter. The resultant filtrate underwent analysis utilizing a UV-visible spectrophotometer, specifically the Shimadzu UV-1800, operating at a designated wavelength of λ = 517 nm. The residual concentration was ascertained by referencing a previously established calibration curve utilizing known concentrations of MR. Subsequently, the removal rate of MR (R_t (%)) and the quantity of MR adsorbed onto the surface of argan nut shells (Q_t (mg/g)) were computed using the ensuing equations (1) and (2):

$$R_t = \frac{C_0 - C_e}{C_0} \times 100 \quad (1)$$

$$Q_t = \frac{(C_0 - C_e)}{m} \times V \quad (2)$$

Where Q_t signifies the adsorption capacity measured in (mg/g). C_0 and C_e refer to the concentrations of MR before and after adsorption, respectively.

2.5 *Adsorption modeling*

2.5.1 *Adsorption kinetics*

To investigate the adsorption process between the dye and argan nut shells, three models were applied to analyze the kinetics of this interaction, including the Pseudo-First-Order model (PFO), the Pseudo-Second-Order model (PSO),[27] and the intraparticle diffusion model.[28] They will provide data on the rate at which adsorption occurs, thus facilitating the understanding of different stages within the interaction and offering a detailed insight into the process of methylene red absorption by argan nut shells.

The pseudo-first-order linear equation (3) below is widely used for the adsorption of the liquid/solid system:

$$\ln(q_e - q_t) = \ln q_e - K_1 t \tag{3}$$

The linear equation (4) of the pseudo-second-order model is expressed as follows:

$$\frac{t}{q_t} = \frac{1}{K_2 q_e^2} + \frac{1}{q_e} t \tag{4}$$

The equation (5) of the intraparticle diffusion model proposed by Weber and Morris[29] is as follows:

$$q_t = K_{int} t^{\frac{1}{2}} + C_i \tag{5}$$

In this context, q_t represents the amount of methyl red adsorbed at time t (mg/g), while q_e signifies the amount adsorbed at equilibrium (mg/g). The pseudo-first-order rate constant is denoted by K_1 (1/min), and t indicates time (min). For the pseudo-second-order model, K_2 is the rate constant (g/mg·min) reflecting the adsorption speed. Additionally, K_{int} represents the intraparticle diffusion rate constant (mg/g·min$^{1/2}$). Finally, (C_i) is a constant that denotes the thickness of the boundary layer, impacting the diffusion rate.

2.5.2 *Adsorption isotherm*

To analyze and understand adsorption isotherms, graphical representations are used to visualize how the adsorbed quantity (q_e) varies at a constant temperature concerning the residual concentration of the adsorbate (C_e) at equilibrium. Additionally, specific mathematical models are employed. Two commonly used models include the Langmuir equation (6),[30] and the Freundlich equation (7).[31] These models mathematically describe the relationships between adsorption and equilibrium concentrations, providing a framework to interpret and predict adsorption behaviors across different systems and experimental conditions.

$$\frac{C_e}{q_e} = \frac{1}{K_1 q_m} + \frac{C_e}{q_m} \tag{6}$$

Here, q_m is the maximum adsorption capacity of the adsorbent (mg/g), representing the theoretical maximum amount of adsorbate that can be adsorbed per unit mass of adsorbent, q_e (mg/g) denotes the amount of adsorbate adsorbed per unit mass of adsorbent at equilibrium (mg/g), K_l: is constant related to the adsorption energy (L/mg), indicating the affinity of the adsorbate for the Langmuir adsorbent and C_e: represents the equilibrium concentration of the adsorbate in the solution (mg/L).

$$\ln(q_e) = \ln(K_f) + \frac{1}{n} \ln(C_e) \tag{7}$$

K_f is the Freundlich constant, indicating the adsorption capacity of the adsorbent ($mg^{(1-n)} \cdot L^n \cdot g^{-1}$), and n is a dimensionless constant that reflects the adsorption intensity.

The term ($1/n$) is a key parameter that indicates the intensity of adsorption and the heterogeneity of the adsorbent surface. Specifically, the value of n reflects how readily the adsorbate adheres to the adsorbent: when $n < 1$, adsorption is favorable and suggests strong interactions; when $n = 1$, it indicates a linear relationship; and when $n > 1$, adsorption becomes less favorable.

2.5.3 *Thermodynamic study*

The standard thermodynamic parameters, including $\Delta G°$ (free energy), $\Delta H°$ (enthalpy), and $\Delta S°$ (entropy), were derived from experiments carried out at various temperatures: 25, 35, 45, and 55 °C. These parameters were obtained by calculating the slope and intercept from the linear plot of $\ln(K_c)$ against $1/T$. The following equation (8) was used in this determination process:

$$\Delta G^\circ = \Delta H^\circ - T\Delta S^\circ = -RT \ln K_c \tag{8}$$

$$\ln(K_c) = -\frac{\Delta H^\circ}{RT} + \frac{\Delta S^\circ}{R} \tag{9}$$

$$\text{With } K_c = \frac{C_{ads}}{C_e} \tag{10}$$

K_c represents the equilibrium between the concentration of the adsorbate on the surface of the solid C_{ads} and the concentration of the adsorbate in the solution C_e. Additionally, R denotes the gas constant (8.314 $J \cdot mol^{-1} \cdot K^{-1}$), and T represents the absolute temperature (K).

3. Results and discussion

3.1 *Absorbent characterization*

3.1.1 *Analysis using FTIR*

The FTIR spectrum of argan nut shells, presented in Figure 3, shows several characteristic bands corresponding to different functional groups. The broad band at 3,412 cm^{-1} is assigned to O-H stretching, typically associated with hydroxyl group, alcohols, or adsorbed water,[32] which may act as potential hydrogen bonding sites during dye adsorption. The peak at 2,918 cm^{-1} is attributed to C-H stretching of alkyl groups (CH_3 or CH_2) confirming the presence of a lignocellulosic backbone.[33] The band at 1,742 cm^{-1} corresponds to C=O stretching vibrations from acetyl and ester groups of hemicellulose,[34] which can provide active sites for electrostatic interactions with dye molecules. In the region between 1,620 and 1,425 cm^{-1}, peaks correspond to aromatic C=C stretching and carbonyl C=O vibrations.[35] The intense peak at 1,043 cm^{-1} indicates C-O stretching in polysaccharides.[36] Finally, the band at 607 cm^{-1} is associated with in-plane deformation of cyclic structures, which may further enhance adsorption through hydrogen bonding.[37] This FTIR spectrum thus suggests the presence of various organic functional groups and inorganic components in ANSs.

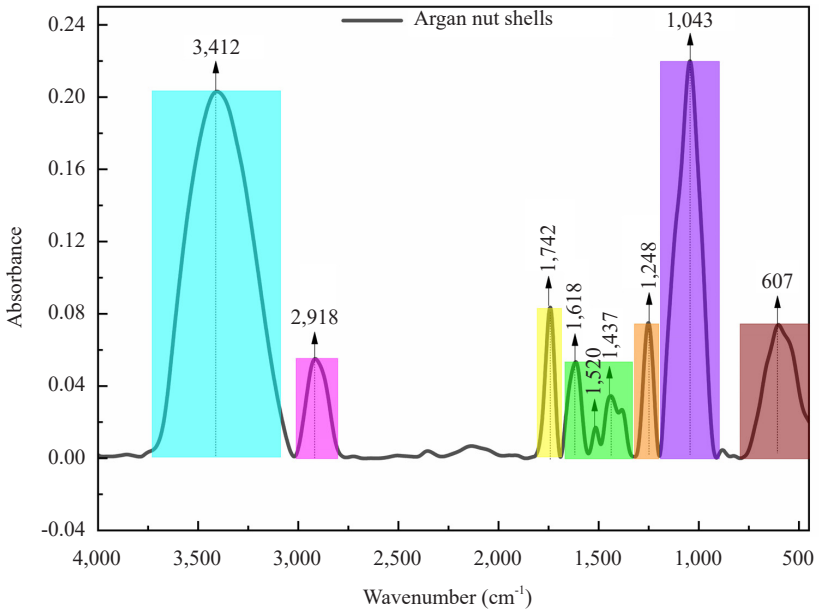

Figure 3. FTIR spectrum of argan nut shells

3.1.2 *X-ray diffraction analysis*

The X-Ray Diffraction (XRD) spectrum of argan nut shells, presented in Figure 4, shows a broad diffuse band and a few poorly defined peaks, indicating a predominantly amorphous structure. The peaks located at 16.3° and 21.9° (2θ) are characteristic of crystalline materials, such as cellulose, present in the nut shells.[38]

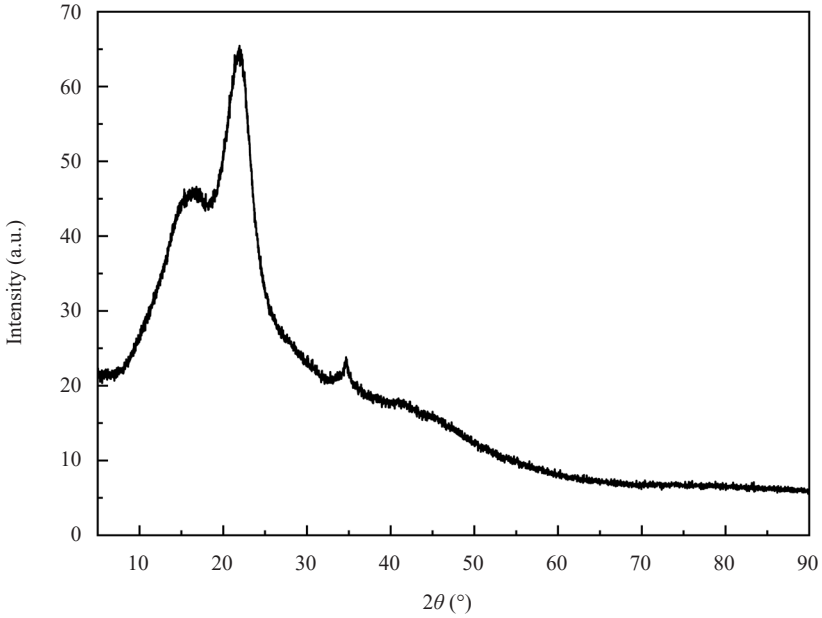

Figure 4. XRD pattern of argan nut shells

The absence of sharp and well-defined peaks in this region suggests a low degree of crystallinity, which is typical

of natural biopolymers, such as lignocelluloses, that form the matrix of plant cell walls. Regarding the crystalline phase, additional hydroxyl groups form numerous hydrogen bonds, creating an extensive network that significantly contributes to the compact crystalline structure.

3.1.3 *SEM/EDS*

The SEM image (Figure 5) of argan nut shells shows a complex and irregular fibrous structure, typical of lignocellulosic biomass. Such entangled fibers suggest the presence of pores and cavities, which increase the available surface area and facilitate the diffusion of adsorbate molecules. This porosity is a crucial property for adsorption processes, as it enhances contact between functional groups and pollutants. The heterogeneous microstructure is due to the presence of compounds like cellulose, hemicellulose, and lignin, which contribute both to structural rigidity and to diversity of active sites.

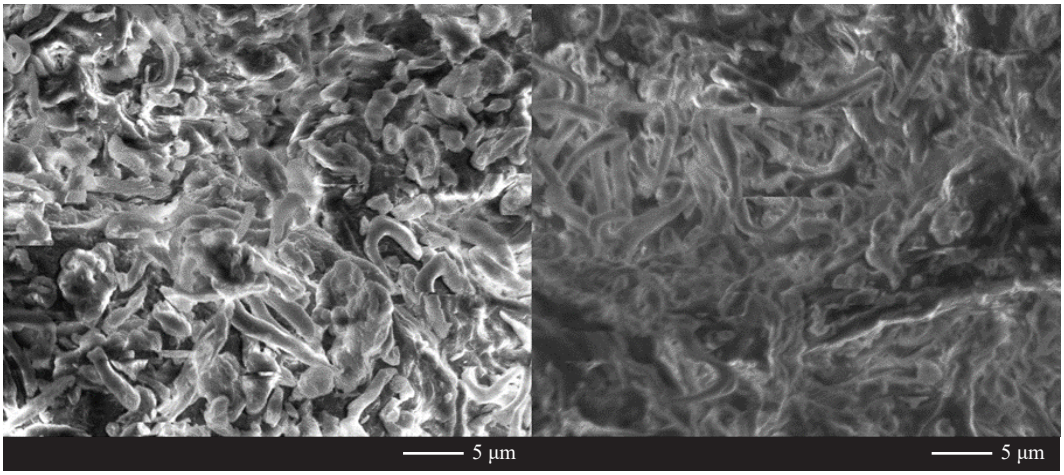

Figure 5. SEM images of argan nut shells

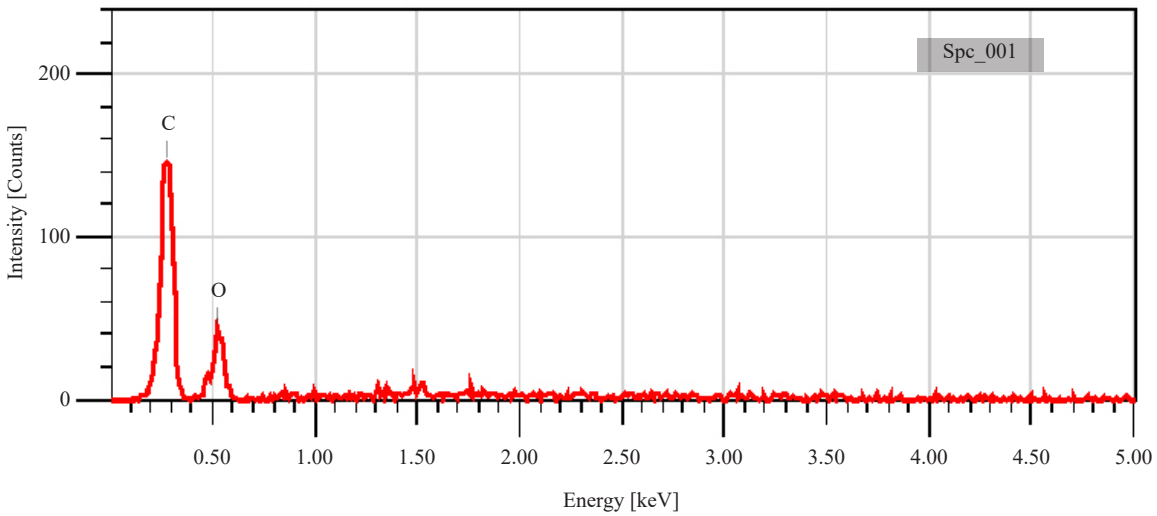

Figure 6. EDS spectrum of argan nut shells

Regarding the EDS spectrum (Figure 6), two major peaks corresponding to Carbon (C) and Oxygen (O) are

observed, confirming the organic composition of these shells. These elements are typically associated with hydroxyl, carboxyl, and aromatic groups present in cellulose and lignin. The predominant presence of carbon and oxygen is also consistent with the lignocellulosic nature of the analyzed material.

3.1.4 *Determination of the pH at the Point of Zero Charge (pH_{PZC})*

The determination of the zero-charge point (pH_{PZC}) of argan nut shells, which corresponds to the pH at which the surface of the adsorbent has no net charge, was carried out (Figure 7). According to the graph, the pH_{PZC} of argan nut shells is 3.68. At this pH, the surface of the material is electrically neutral, meaning it neither attracts cations nor anions. When the pH of the solution is below this value, the surface of the adsorbent is positively charged, favoring the adsorption of anions. Conversely, when the pH is above 3.68, the surface becomes negatively charged, promoting the adsorption of cations. This parameter is essential for understanding and optimizing the effectiveness of argan nut shells as an adsorbent in water treatment applications or other adsorption fields.

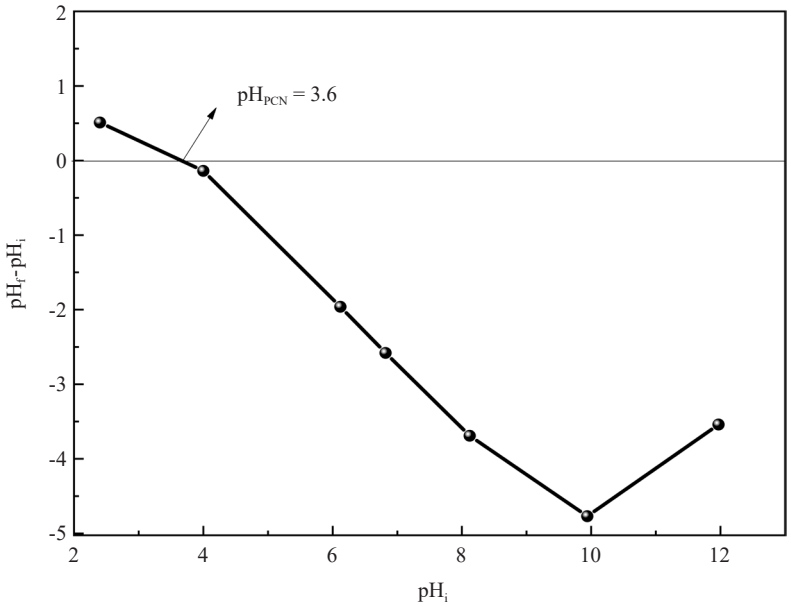

Figure 7. Point zero charge for argan nut shells

3.2 *Adsorption of MR on argan nut shells*

3.2.1 *Effect of pH*

Initial pH plays a critical role in the removal process of methyl red. To investigate the effect of pH on dye adsorption, the initial pH was varied from 2 to 12, maintaining a dye concentration of 30 mg/L, a temperature of 25 °C, and an adsorbent mass of 80 mg. Figure 8 shows the amount (mg) of dye adsorbed per gram of adsorbent according to the initial pH.

Results demonstrate a clear relationship between initial pH and the adsorption of methyl red by argan nut shells. At pH values below 4, where the adsorbent surface is positively charged, a significant amount of dye is adsorbed (4.9 mg at pH 2). This can be explained by the strong electrostatic attraction between the oppositely charged surface and dye molecules. However, as the pH increases beyond the point of zero charge (pH 4), the adsorbed quantity progressively decreases because the surface becomes negatively charged, hindering the adsorption of the cationic dye. This decline is more pronounced at higher pH levels (8, 10, 12), indicating a drastic reduction in electrostatic interactions between the dye and the negatively charged surface. For instance, the bark of hopbush has been reported to show a decrease in adsorption capacity with increasing pH under similar conditions.[39]

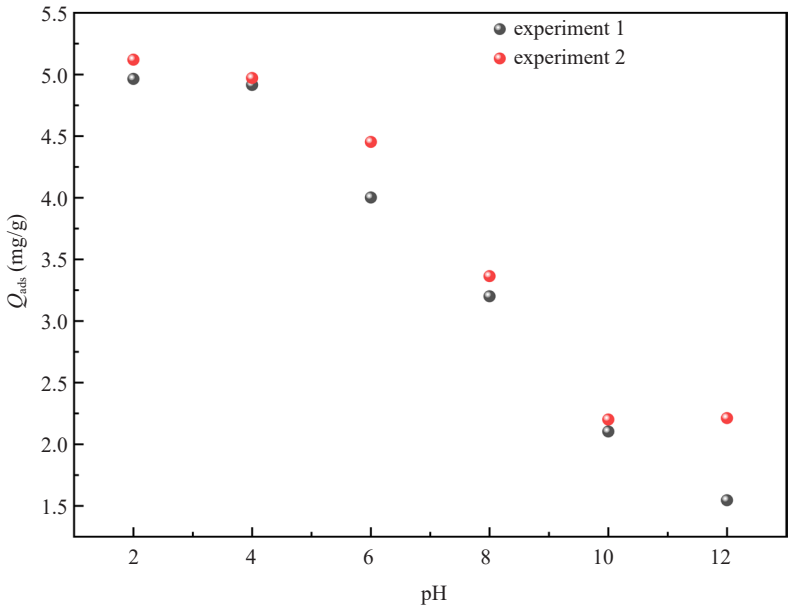

Figure 8. Effect of pH on methyl red adsorption

3.2.2 *Effect of adsorbent mass*

In most studies concerning the adsorption phenomenon, the amount of adsorbent has a considerable impact on the adsorption efficiency.[40] To investigate this effect, various masses of Argan Nut Shells (ANS), ranging from 10 mg to 100 mg, were brought in contact with 20 mL aqueous solution of Methyl Red (MR) at 30 mg/L.

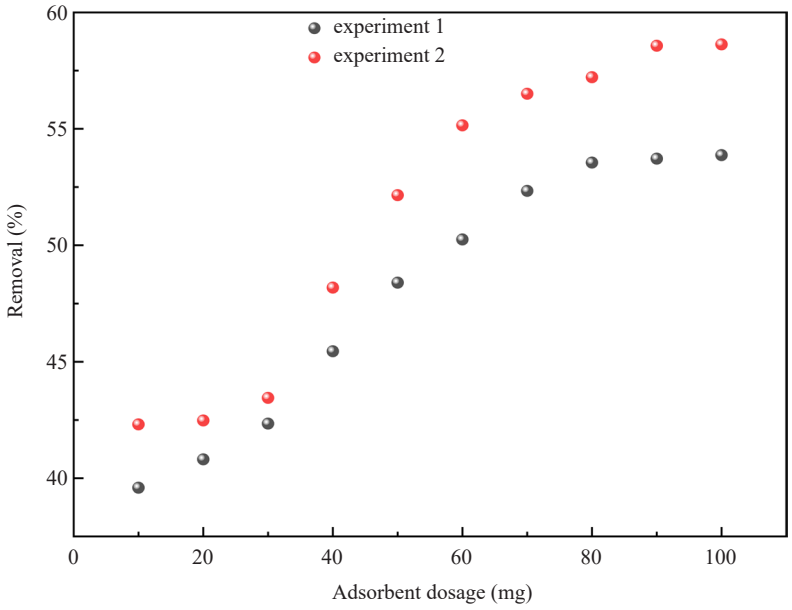

Figure 9. Effect of adsorbent mass on methyl red adsorption

Figure 9 highlights an increase in the rate of MR removal as a function of increasing adsorbent quantity. This

trend can be attributed to the increase of the sorption-friendly surface and the increased availability of active adsorption sites.[41] The maximum removal efficiency ANS reached 53.5% at 80 mg. While this performance may appear modest, it remains comparable to other agricultural waste-derived adsorbents. For instance, rice husk has been reported to remove 48–55% of methyl red under similar conditions,[42] whereas the mucilage of salvia seed achieved about 34–54% for azo dyes.[43] Given the abundance and very low cost of ANS, their adsorption efficiency is competitive, particularly when considering the added ecological benefit of valorizing argan byproducts.

3.2.3 *Adsorption kinetics of MR on argan nut shells*

The kinetic representation of MR adsorption on ANS, shown in Figure 10, illustrates the vibration of the adsorbed quantity as a function of agitation time. This curve reveals a steady increase in the adsorbed quantity until it reaches a plateau, indicating the establishment of an adsorption equilibrium as the process evolves.[44] This equilibrium point is achieved within 80 minutes, demonstrating a stabilized adsorption capacity at 6.7 mg/g. Initially, adsorption rapidly increases, driven by the accumulation of MR at the active surface sites of the adsorbent, sites that remain available for this interaction.[45] It should be noted that ANS suspensions formed stable dispersions under the experimental conditions, which ensured consistent adsorption kinetics and reproducibility. However, the slower growth observed in a later stage is attributed to the diffusion of the dye into the pores of the adsorbent, as the external adsorption sites are fully occupied at this stage. [46] This alteration in the adsorption kinetics showcases the complex evolution of the process, transitioning from an initial rapid adsorption phase to a stage where diffusion into porous structures becomes predominant as surface sites become saturated.

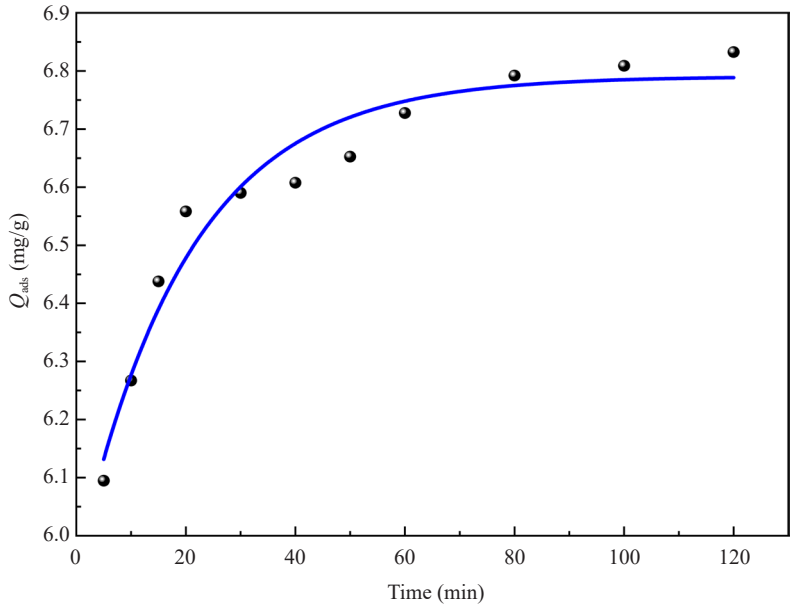

Figure 10. Impact of contact time on methyl red adsorption

To study the adsorption rate of MR on ANS, three kinetic models were employed: the pseudo-first-order kinetic model, the pseudo-second-order kinetic model, and the intraparticle diffusion model. These models contribute to elucidating the process through which the adsorbate is adsorbed onto the surface of the adsorbent.[47]

3.2.3.1 *Pseudo-first-order kinetic models*

The graph of $\ln(q_e - q_t)$ as a function of (t), as illustrated in Figure 11, corresponds to the Pseudo-First-Order (PFO) kinetic model. This model presents a linear evolution (red line) that does not fit well with the experimental data points,

since the regression factor R^2 is almost low (0.972). This indicates that the kinetics of MR adsorption on ANS deviates from the pseudo-first-order kinetic model.

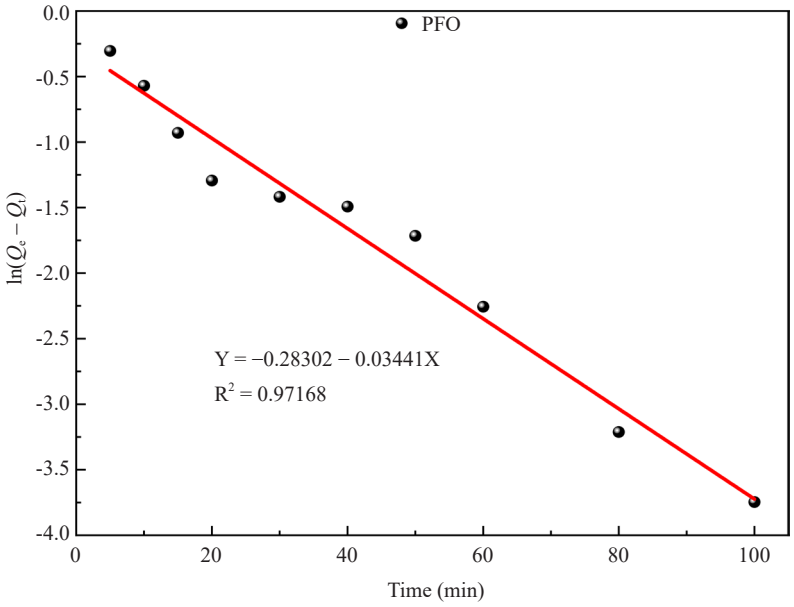

Figure 11. PFO model for methyl red adsorption

3.2.3.2 *Pseudo-second-order model*

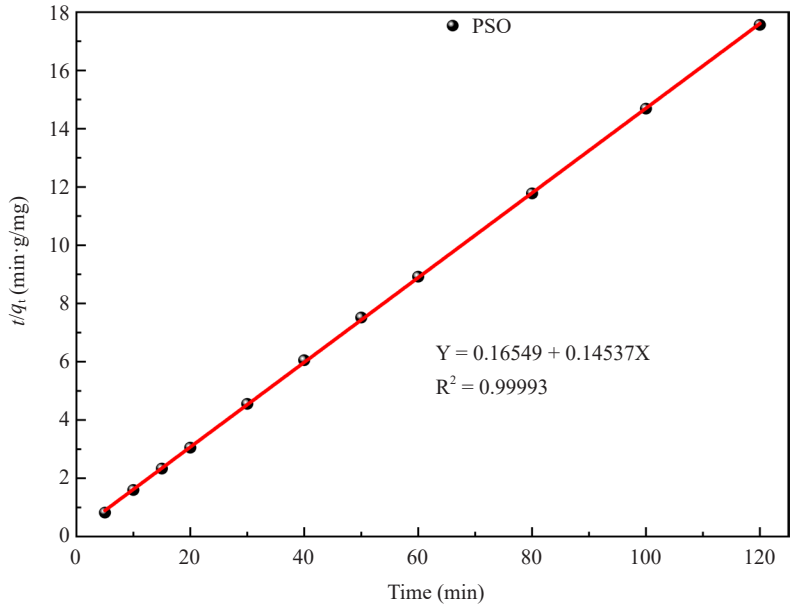

Figure 12. PSO model for methyl red adsorption

The pseudo-second-order kinetic model is presented in Figure 12, showing the evolution of the t/q_t ratio as a

function of time. The fitting of the curve resulted in a correlation coefficient (R^2) of 0.999. From this plot, the parameters K_2 and q_e were determined as 0.127 g/mg·min and 6.878 mg/g, respectively, as listed in Table 1. The close agreement between the calculated q_e (6.878 mg/g) and the experimental value (6.832 mg/g) confirms that the adsorption of MR onto ANS follows the pseudo-second-order kinetic model with high accuracy.

Table 1. Values of kinetic parameters in the PFO and PSO models concerning the adsorption of methyl red onto Argan Nut Shells (ANS)

Adsorbent	Q_{exp} (mg/g)	Lagergren (Pseudo-first-order)			Ho and Coll (Pseudo-second-order)		
		K_1 (min^{-1})	Q_{cal} (mg/g)	R^2	K_2 (g/mg·min)	Q_{cal} (mg/g)	R^2
ANS	6.832	0.034	6.753	0.972	0.127	6.879	0.999

3.2.3.3 *Intra-particle diffusion model*

The intra-particle diffusion model is shown in Figure 13 and reveals two distinct phases in the diffusion pathway of MR onto ANS. The first, fast phase corresponds to the migration of molecules to the migration of molecules to the external surface of the adsorbent, while the second, slower phase reflects the approach to adsorption equilibrium.[48] If intra-particle diffusion were the sole rate-limiting step, the curve would pass through the origin. However, the plot in Figure 13 deviates from this expectation, indicating that other processes also influence the adsorption rate. The different parameters obtained from this model are listed in Table 2.

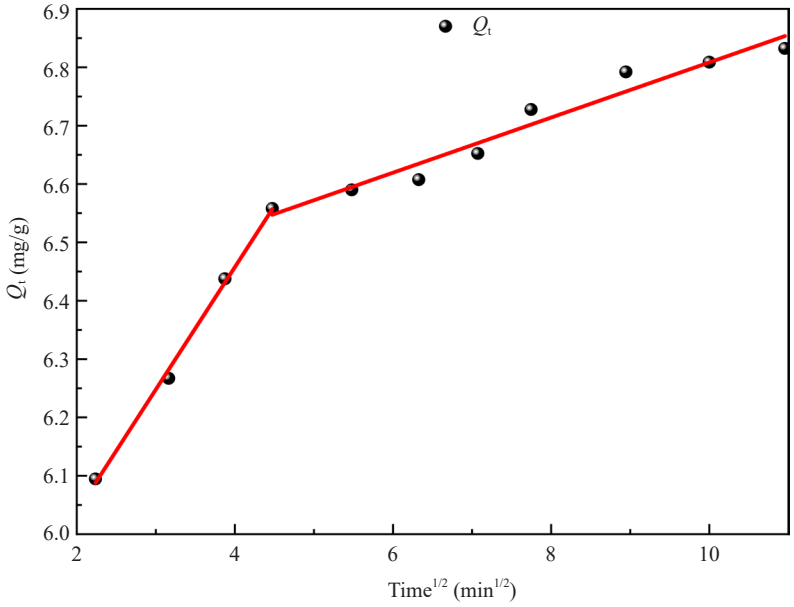

Figure 13. Intra-particle diffusion model for methyl red adsorption

Table 2. Parameters of the intra-particle diffusion model for the adsorption of methyl red on Argan Nut Shells (ANS)

Adsorbent	Weber and Morris[29]					
	Step 1			Step 2		
	K_{int} (mg/g·min$^{1/2}$)	C_1	R^2	K_{int} (mg/g·min$^{1/2}$)	C_2	R^2
ANS	0.209	5.618	0.997	0.047	6.336	0.957

3.2.4 *Adsorption isotherm of MR on argan nut shells*

To further investigate the adsorption of MR onto argan nut shells, adsorption isotherms were established at 25 °C, covering various concentrations of MR. The Langmuir and Freundlich models aimed to elucidate the nature of these isotherms, the maximum adsorption capacity, and the potential mechanisms of interactions between the adsorbent and the dye. These isotherms are graphically represented in Figure 14. They highlight significant disparities in the adsorption of MR onto ANS. Analysis of the experimental data using the Langmuir and the Freundlich models confirmed these differences. Specifically, the Freundlich model exhibited close correspondence with the experimental points, whereas the Langmuir model did not match most of the collected data. The parameters derived from these models are summed up in Table 3. The values recorded in this table indicate that the correlation coefficient R^2 approaches 1 for the Freundlich model, whereas the Langmuir model one is far from 1. This observation leads us to conclude that the Freundlich model provides a more consistent representation of the experimental outcomes regarding the MR adsorption equilibrium onto argan nut shells, thus conforming with previous research findings.

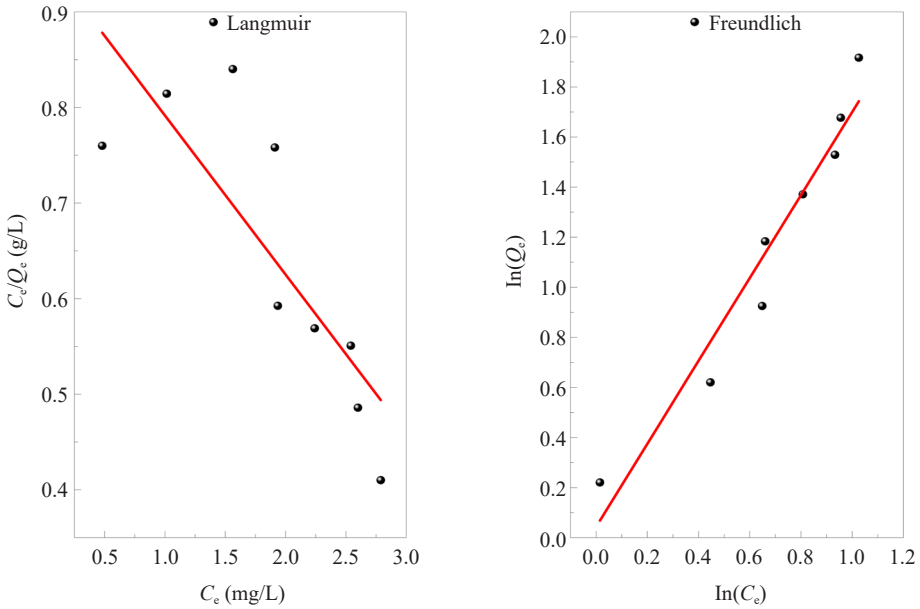

Figure 14. Linear regression of methyl red adsorption isotherms on argan nut shells: Langmuir and Freundlich models

Table 3. Parameters of the Langmuir; Freundlich linear models for methyl red adsorption

Parameters	Langmuir			Freundlich		
	q_m (mg/g)	K_L (L/mg)	R^2	K_F ($mg^{(1-n)}\cdot ln\cdot g^{-1}$)	n	R^2
Values	-6.011	-6.274	0.686	1.044	0.603	0.944

3.3 *Thermodynamic study*

Thermodynamic analysis, depicted in Figure 15 with the plot ln(K_c) versus 1/T, reveals significant variations in the thermodynamic parameters of adsorption on argan nut shells, as detailed in Table 4. At 298 K, the entropy ($\Delta S°$) displays a highly negative value (-91.382 J/K·mol), which reflects a high degree of order at the solid-liquid interface during adsorption. The negative entropy value can be attributed to the reduced randomness and restricted mobility of dye molecules once adsorbed onto the surface, compared to their more dynamic state in aqueous solution. The negative $\Delta H°$ value (-32.8 kJ/mol) indicates an exothermic process. The magnitude of $\Delta H°$ suggests a predominance of physisorption, with possible contributions from chemisorption through interactions between the azo groups of MR and the oxygenated functional sites of ANS. These findings imply that the adsorption process is favorable at ambient conditions, which is particularly advantageous for wastewater treatment applications where additional energy input is undesirable. The negative $\Delta G°$ values at all studied temperatures confirm that MR adsorption onto ANS is spontaneous. However, at higher temperatures (308 K, 318 K, and 328 K), there is a trend towards decreasing $\Delta G°$ values, respectively reaching -4.722 kJ/mol, -3.808 kJ/mol, and -2.894 kJ/mol. Despite becoming less negative, $\Delta G°$ remains negative, suggesting that adsorption continues to be a spontaneous process even with increased temperature. This variation also indicates a change in the adsorption efficiency with respect to temperature. Nevertheless, the process remains favorable under all studied conditions.

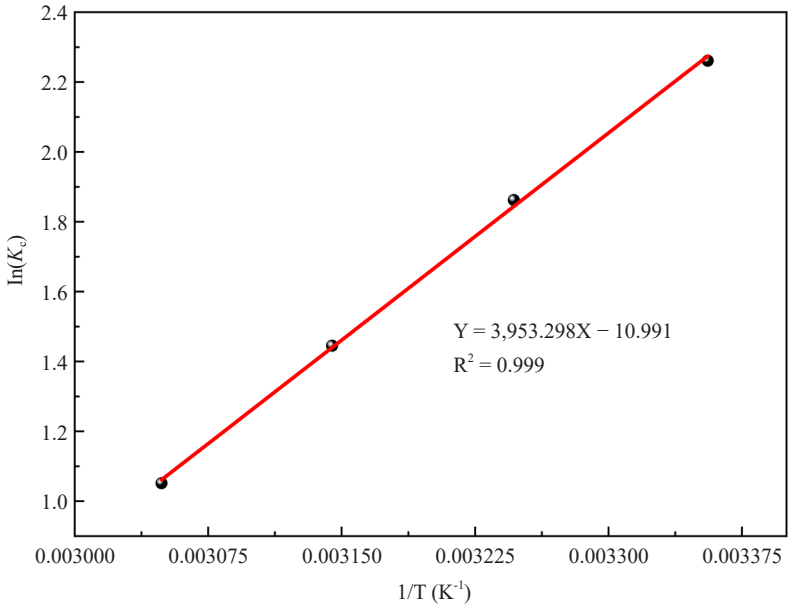

Figure 15. Line of the Van't Hoff equation for the adsorption of methyl red

Table 4. Thermodynamic parameters for methyl red adsorption on argan nut shells

Adsorbent	T (K^{-1})	$\Delta S°$ (J/K·mol)	$\Delta H°$ (kJ/mol)	$\Delta G°$ (kJ/mol)
Argan nut shells	298	-91.382	-32.867	-5.635
	308			-4.722
	318			-3.808
	328			-2.894

3.4 *Mechanism of methyl red adsorption*

The FTIR spectra of argan nut shells before and after the adsorption of methyl red (Figure 16) reveal noticeable spectral changes, highlighting the interactions between the functional groups of the adsorbent and the dye molecules. The broad O-H stretching band initially observed at 3,412 cm^{-1} undergoes a slight shift toward higher wavenumbers, suggesting a transition from a hydrogen-bonded hydroxyl group (within polysaccharides) to a more free hydroxyl group due to interactions with methyl red.

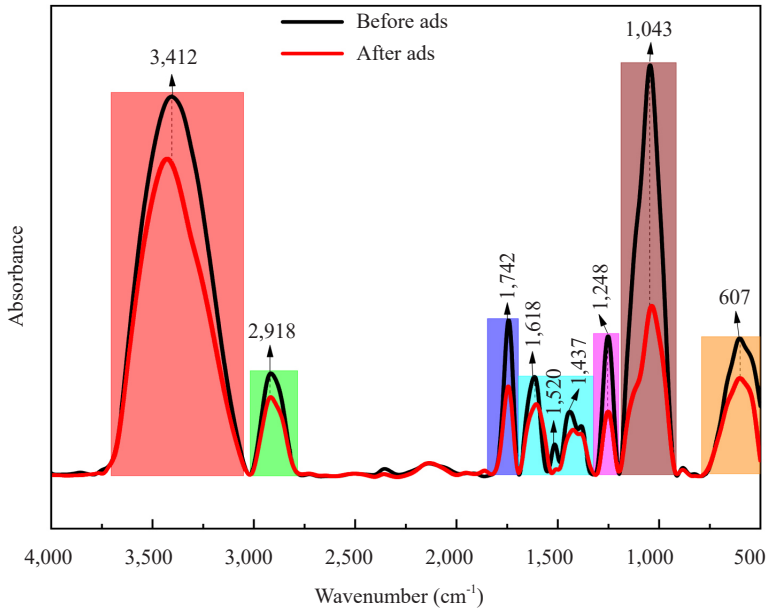

Figure 16. FTIR spectra of argan nut shells before and after methyl red adsorption

A notable decrease in the intensity of the C-H stretching band at 2,918 cm^{-1} indicates the possible involvement of aliphatic chains in the adsorption process. The band at 1,742 cm^{-1}, typically assigned to carbonyl (C=O) stretching vibrations, remains present after adsorption, confirming that it does not correspond to methyl red itself but rather to intrinsic esters or carboxyl groups in argan shells. To ensure accurate analysis, the spectra should be normalized relative to this band.

Significant changes are observed in the aromatic C=C and carboxylate-related vibrations at 1,618 cm^{-1} and 1,437 cm^{-1}, with both shifts in position and intensity variation, suggesting strong π-π interactions between the conjugated systems of methyl red and argan shells. Additionally, the torsional vibration at 607 cm^{-1} exhibits modifications, which

may indicate specific interactions between the azo (-N=N-) groups of methyl red and active adsorption sites on the argan shells.

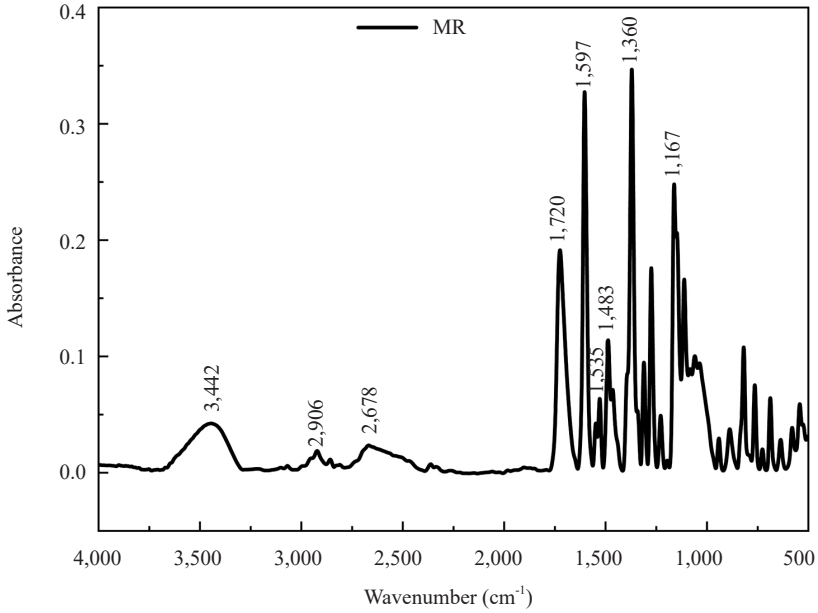

Figure 17. FTIR spectrum of methyl red

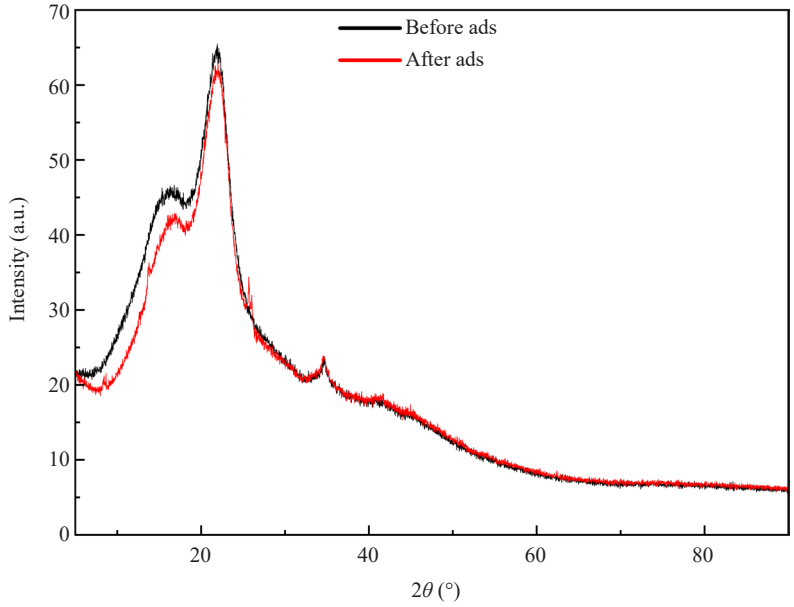

Figure 18. Diffractograms of argan nut shells before and after methyl red adsorption

It is also important to verify the presence of characteristic peaks of methyl red by analyzing its independent FTIR spectrum (Figure 17). The spectrum (methyl red) does not exhibit a band at 1,742 cm^{-1}, confirming that this peak is not associated with the dye. Further analysis of small shifts in key bands (e.g., hydroxyl group and aromatic regions) could

provide deeper insights into the adsorption mechanism. These spectral modifications suggest that hydrogen bonding and π-π stacking interactions between MR molecules and the aromatic or oxygenated functional groups of ANS. Although the FTIR evidence remains indirect, the normalization strengthens the mechanistic interpretation, suggesting that multiple non-covalent interactions act synergistically to drive adsorption.

The diffractograms of argan nut shells before and after dye adsorption are presented in Figure 18. They show a remarkable similarity, suggesting that the material undergoes no significant alteration following this interaction with the dye. This similarity between the diffractograms indicates that the crystalline structure or arrangement of the material's components remains fundamentally unchanged after dye adsorption. This suggests that the dye adsorption did not induce major modifications in the arrangement of particles or the crystalline structure of the argan nut shells, at least not at a scale detectable by X-ray diffraction.

4. Conclusions

The study confirms the potential of argan nut shells as a sustainable and low-cost adsorbent for the removal of methyl red. The adsorption process followed a pseudo-second-order kinetic model and was best described by the Freundlich isotherm, with thermodynamic parameters indicating spontaneity and exothermicity under ambient conditions. Surface analyses (FTIR, XRD, SEM, and EDS) verified interactions between MR molecules and the functional groups of ANS.

Furthermore, the maximum removal efficiency (53.5%) is moderate compared with activated or chemically modified adsorbents; however, ANS remain competitive due to their abundance, negligible cost, and environmental value as an underutilized biomass. The main limitations of this study are the absence of specific surface area and pore structure measurements by the BET method, due to the unavailability of the required equipment, and the use of distilled water instead of real effluents. Future research should address these limitations by incorporating surface area and porosity analyses, exploring surface modification or composite development, and testing ANS in complex wastewater systems to enhance performance and applicability.

By valorizing argan residues for wastewater treatment, this work contributes to sustainable dye remediation strategies and supports a circular economy approach in regions where argan oil production is significant.

Conflict of interest

The authors declare that there is no conflict of interest

References

[1] Dutta, S.; Adhikary, S.; Bhattacharya, S.; Roy, D.; Chatterjee, S.; Chakraborty, A.; Banerjee, D.; Ganguly, A.; Nanda, S.; Rajak, P. Contamination of textile dyes in aquatic environment: adverse impacts on aquatic ecosystem and human health, and its management using bioremediation. *J. Environ. Manage.* **2024,** *353*, 120103. https://doi.org/10.1016/j.jenvman.2024.120103.

[2] Berradi, M.; Hsissou, R.; Khudhair, M.; Assouag, M.; Cherkaoui, O.; El Bachiri, A.; El Harfi, A. Textile finishing dyes and their impact on aquatic environs. *Heliyon* **2019,** *5*(11), e02711. https://doi.org/10.1016/j.heliyon.2019.e02711.

[3] Sharma, K.; Chakroborty, S.; Pal, K.; Panda, A. R.; Malviya, J.; Nath, N.; Yadav, T.; Parmar, A. S.; Parmar, L.; Asthana, N.; et al. Controllable synthesis of high-yield magnetic nanomaterials assisted dye adsorbents from waste-water treatment and applications. *J. Mol. Struct.* **2024,** *1304*, 137550. https://doi.org/10.1016/j.molstruc.2024.137550.

[4] Ikram, M.; Naeem, M.; Zahoor, M.; Rahim, A.; Hanafiah, M. M.; Oyekanmi, A. A.; Shah, A. B.; Mahnashi, M. H.; Al Ali, A.; Jalal, N. A.; et al. Biodegradation of azo dye methyl red by *Pseudomonas aeruginosa*: optimization of process conditions. *Int. J. Environ. Res. Public Health* **2022,** *19*(16), 9962. https://doi.org/10.3390/ijerph19169962.

[5] Behera, U. S.; Poddar, S.; Byun, H. S. Maximizing methyl red dye removal efficiency: a targeted parameter

approach. *J. Chem. Technol. and Biotechnol.* **2024,** *99*(5), 1212-1224. https://doi.org/10.1002/jctb.7626.
[6] Kishor, R.; Purchase, D.; Saratale, G. D.; Ferreira, L. F. R.; Bilal, M.; Iqbal, H. M. N.; Bharagava, R. N. Environment friendly degradation and detoxification of Congo red dye and textile industry wastewater by a newly isolated *Bacillus cohnni* (RKS9). *Environ. Technol. Innov.* **2021,** *22*, 101425. https://doi.org/10.1016/j.eti.2021.101425.
[7] Sharma, A.; Singh, S. K.; Nath, A.; Sundaram, S. Methyl red biodegradation by novel halophilic *Lactiplantibacillus plantarum* SS-AU1 isolated from River Ganges. *Int. J. Environ. Sci. Technol.* **2024,** *21*, 7191-7206. https://doi.org/10.1007/s13762-024-05468-0.
[8] Irwan, I.; Jumbi, I. S.; Alimin, A.; Ratna, R.; Nohong, N.; Maulidiyah, M.; Nurdin, M.; Muzakkar, M. Z. Electrochemical photodegradation of methyl red using reduced graphene oxide of palm shells supported TiO_2 nanoparticle under visible irradiation. *Anal. Bioanal. Electrochem.* **2023,** *15*(7), 556-567. https://doi.org/10.22034/abec.2023.706509.
[9] Ullah, I.; Tariq, M.; Muhammad, M.; Khan, J.; Rahim, A.; Abdullah, A. Z. UV photocatalytic remediation of methyl red in aqueous medium by sulfate ($SO_4^{\bullet-}$) and hydroxyl (•OH) radicals in the presence of Fe^{2+} and Co@ TiO_2 NPs photocatalysts. *Colloids Surf. A Physicochem. Eng. Asp.* **2023,** *679*, 132614. https://doi.org/10.1016/j.colsurfa.2023.132614.
[10] Nagshbandi, Z.; Gholinejad, M.; Sansano, J. M. Novel magnetic zeolitic imidazolate framework for room temperature enhanced catalysis. *Inorg. Chem. Com.* **2023,** *150*, 110463. https://doi.org/10.1016/j.inoche.2023.110463.
[11] Kouakou, L. P. M. S.; Karidioula, D.; Manouan, M. R. W.; Pohan, A. G. L.; Cissé, G.; Konan, L. K.; Andji-Yapi, J. Y. Use of two clays from Côte d'Ivoire for the adsorption of methyl red from aqueous medium. *Chem. Phys. Lett.* **2023,** *810*, 140183. https://doi.org/10.1016/j.cplett.2022.140183.
[12] Saeed, T.; Naeem, A.; Din, I. U.; Farooq, M.; Khan, I. W.; Hamayun, M.; Malik, T. Synthesis of chitosan composite of metal–organic framework for the adsorption of dyes: kinetic and thermodynamic approach. *J. Hazard Mater.* **2022,** *427*, 127902. https://doi.org/10.1016/j.jhazmat.2021.127902.
[13] Shahinpour, A.; Tanhaei, B.; Ayati, A.; Beiki, H.; Sillanpää, M. Binary dyes adsorption onto novel designed magnetic clay–biopolymer hydrogel involves characterization and adsorption performance: kinetic, equilibrium, thermodynamic, and adsorption mechanism. *J. Mol. Liq.* **2022,** *366*, 120303. https://doi.org/10.1016/j.molliq.2022.120303.
[14] Sadoq, M.; Atlas, H.; Imame, S.; Kali, A.; Amar, A.; Loulidi, I.; Jabri, M.; Sadoq, B. E.; Ouchabi, M.; Sannasi, P.; et al. Elimination of crystal violet from aqueous solution by adsorption on natural polysaccharide: kinetic, isotherm, thermodynamic studies and mechanism analysis. *Arabian J. Chem.* **2024,** *17*(1), 105453. https://doi.org/10.1016/j.arabjc.2023.105453.
[15] Romdhane, D. F.; Satlaoui, Y.; Nasraoui, R.; Charef, A.; Azouzi, R. Adsorption, modeling, thermodynamic, and kinetic studies of methyl red removal from textile-polluted water using natural and purified organic matter-rich clays as low-cost adsorbent. *J. Chem.* **2020,** *2020*, 4376173. https://doi.org/10.1155/2020/4376173.
[16] Amar, A.; Loulidi, I.; Kali, A.; Boukhlifi, F.; Hadey, C.; Jabri, M. Physicochemical characterization of regional clay: application to phenol adsorption. *Appl. Environ. Soil Sci.* **2021,** *2021*, 8826063. https://doi.org/10.1155/2021/8826063.
[17] Deshmukh, S.; Topare, N. S.; Raut-Jadhav, S.; Thorat, P. V.; Bokil, S. A.; Khan, A. Orange peel activated carbon produced from waste orange peels for adsorption of methyl red. *Aqua Water Infrastruct. Ecosyst. Soc.* **2022,** *71*(12), 1351-1363. https://doi.org/10.2166/aqua.2022.119.
[18] Nizam, N. U. M.; Hanafiah, M. M.; Mahmoudi, E.; Halim, A. A.; Mohammad, A. W. The removal of anionic and cationic dyes from an aqueous solution using biomass-based activated carbon. *Sci. Rep.* **2021,** *11*, 8623. https://doi.org/10.1038/s41598-021-88084-z.
[19] Gohr, M. S.; Abd-Elhamid, A. I.; El-Shanshory, A. A.; Soliman, H. M. A. Adsorption of cationic dyes onto chemically modified activated carbon: kinetics and thermodynamic study. *J. Mol. Liq.* **2022,** *346*, 118227. https://doi.org/10.1016/j.molliq.2021.118227.
[20] Ioannou, Z.; Karasavvidis, C.; Dimirkou, A.; Antoniadis, V. Adsorption of methylene blue and methyl red dyes from aqueous solutions onto modified zeolites. *Water Sci. and Technol.* **2013,** *67*(5), 1129-1136. https://doi.org/10.2166/wst.2013.672.
[21] Mubarak, M. F.; Mohamed, A. M. G.; Keshawy, M.; elMoghny, T. A.; Shehata, N. Adsorption of heavy metals and hardness ions from groundwater onto modified zeolite: Batch and column studies. *Alexandria Engin. J.* **2022,** *61*(6), 4189-4207. https://doi.org/10.1016/j.aej.2021.09.041.
[22] El Khomri, M.; El Messaoudi, N.; Dbik, A.; Bentahar, S.; Lacherai, A. Efficient adsorbent derived from *Argania*

spinosa for the adsorption of cationic dye: Kinetics, mechanism, isotherm and thermodynamic study. *Surf. Interfaces* **2020,** *20*, 100601. https://doi.org/10.1016/j.surfin.2020.100601.
[23] Qamouche, K.; Chetaine, A.; El Yahyaoui, A.; Moussaif, A.; Fröhlich, P.; Bertau, M.; Haneklaus, N. Uranium and other heavy metal sorption from Moroccan phosphoric acid with argan nutshell sawdust. *Miner. Eng.* **2021,** *171*, 107085. https://doi.org/10.1016/j.mineng.2021.107085.
[24] Kataya, G.; Cornu, D.; Bechelany, M.; Hijazi, A.; Issa, M. Biomass waste conversion technologies and its application for sustainable environmental development—A review. *Agronomy*. **2023,** *13*(11), 2833. https://doi.org/10.3390/agronomy13112833.
[25] Al-Qahtani, S. D.; Alhasani, M.; Alkhathami, N.; Abu Al-Ola, K. A.; Alkhamis, K.; El-Desouky, M. G.; El-Bindary, A. A. Effective levofloxacin adsorption and removal from aqueous solution onto tea waste biochar: Synthesis, characterization, adsorption studies, and optimization by Box–Behnken design and its antibacterial activity. *Environ. Technol.* **2024,** *45*(23), 4928-4950. https://doi.org/10.1080/09593330.2023.2283409.
[26] Ahamad, Z.; Ahmed, M.; Mashkoor, F.; Nasar, A. Chemically modified *Azadirachta indica* sawdust for adsorption of methylene blue from aqueous solutions *Biomass Convers. Biorefin.* **2024,** *14*, 19929-19946. https://doi.org/10.1007/s13399-023-04161-5.
[27] Şenol, Z. M.; Messaoudi, N. El; Fernine, Y.; Keskin, Z. S. Bioremoval of rhodamine B dye from aqueous solution by using agricultural solid waste (almond shell): Experimental and DFT modeling studies. *Biomass Convers. Biorefin.* **2024,** *14*, 17927-17940. https://doi.org/10.1007/s13399-023-03781-1.
[28] Pashchenko, D. Intra-particle diffusion limitation for steam methane reforming over a Ni-based catalyst. *Fuel* **2023,** *353*, 129205. https://doi.org/10.1016/j.fuel.2023.129205.
[29] Morris, J. C.; Weber, J. W. J. Removal of biologically-resistant pollutants from waste waters by adsorption. In *Advances in Water Pollution Research: Proceedings of the International Conference Held in London*; Elsevier: London, 1964; pp 231-266. https://doi.org/10.1016/B978-1-4832-8391-3.50032-4.
[30] Ezzati, R.; Ezzati, S.; Azizi, M. Exact solution of the Langmuir rate equation: New insights into pseudo-first-order and pseudo-second-order kinetics models for adsorption. *Vacuum* **2024,** *220*, 112790. https://doi.org/10.1016/j.vacuum.2023.112790.
[31] Pereira, S. K.; Kini, S.; Prabhu, B.; Jeppu, G. P. A simplified modeling procedure for adsorption at varying pH conditions using the modified Langmuir–Freundlich isotherm. *Appl. Water Sci.* **2023,** *13*, 29. https://doi.org/10.1007/s13201-022-01800-6.
[32] Blindheim, F. H.; Ruwoldt, J. The effect of sample preparation techniques on lignin Fourier transform infrared spectroscopy. *Polymers* **2023,** *15*(13), 2901. https://doi.org/10.3390/polym15132901.
[33] Meng, P.; Huang, J.; Yang, Z.; Jiang, M.; Wang, Y.; Zhang, W.; Zhang, J.; Sun, B.; Fu, C. Air-stable binary hydrated eutectic electrolytes with unique solvation structure for rechargeable aluminum-ion batteries. *Nano. Micro. Lett.* **2023,** *15*, 188. https://doi.org/10.1007/s40820-023-01160-z.
[34] Halloub, A.; Raji, M.; Essabir, H.; Kassab, Z.; Boussen, R.; Chakchak, H.; Bensalah, M. O.; El Achaby, M.; Bouhfid, R.; Qaiss, A. El Kacem. Production and characterization of rectangular cellulose nanocrystals (type II) from nutshells: Argan nutshells (ANS) as a case study. *Biomass Convers. Biorefin.* **2023,** *14*, 29079-29090. https://doi.org/10.1007/s13399-023-04164-2.
[35] El Ouahabi, H.; Elmouwahidi, A.; Cano-Casanova, L.; Lillo-Ródenas, M. Á.; Roman-Martínez, M. C.; Pérez-Cadenas, A. F.; Bailón-García, E.; Shaban, M.; Al-Senani, G. M.; Ouzzine, M.; Khaddor, M. From nutshells to energy cells: Pioneering supercapacitor electrodes via innovative argan nutshell activated carbon synthesis. *J. Energy Storage* **2024,** *82*, 110598. https://doi.org/10.1016/j.est.2024.110598.
[36] Thombare, N.; Mahto, A.; Singh, D.; Chowdhury, A. R.; Ansari, M. F. Comparative FTIR characterization of various natural gums: A criterion for their identification. *J. Polym. Environ.* **2023,** *31*, 2272-2280. https://doi.org/10.1007/s10924-023-02821-1.
[37] Abou-Hadid, A. F.; El-Behairy, U. A.; Elmalih, M. M.; Amdeha, E.; Naggar, A. M. A. E.; Taha, M. H.; Hussein, A. E. M. Conversion of corn shell as biomass solid waste into carbon species for efficient decontamination of wastewater via heavy metals adsorption. *Biomass Convers. Biorefin.* **2024,** *14*, 16435-16449. https://doi.org/10.1007/s13399-023-04057-4.
[38] Shaheed, N.; Javanshir, S.; Esmkhani, M.; Dekamin, M. G.; Naimi-Jamal, M. R. Synthesis of nanocellulose aerogels and Cu-BTC/nanocellulose aerogel composites for adsorption of organic dyes and heavy metal ions. *Sci. Rep.* **2021,** *11*, 18553. https://doi.org/10.1038/s41598-021-97861-9.
[39] Gul, S.; Kanwal, M.; Qazi, R. A.; Gul, H.; Khattak, R.; Khan, M. S.; Khitab, F.; Krauklis, A. E. Efficient removal of methyl red dye by using bark of hopbush. *Water* **2022,** *14*(18), 2831. https://doi.org/10.3390/w14182831.
[40] Abin-Bazaine, A.; Campos Trujillo, A.; Olmos-Marquez, M. Adsorption isotherms: enlightenment of

the phenomenon of adsorption. In *Waste water Treatment*; IntechOpen, 2022. https://doi.org/10.5772/intechopen.104260.

[41] Malini, K.; Selvakumar, D.; Kumar, N. S. Activated carbon from biomass: Preparation, factors improving basicity and surface properties for enhanced CO_2 capture capacity—A review. *J. CO_2 Util.* **2023,** *67*, 102318. https://doi.org/10.1016/j.jcou.2022.102318.

[42] Mat Jidin, M. A. S.; Jani, M.; Mohd Fauzi, N.; Subki, N. S. Removal of methyl red in wastewater by activated carbon derived from rice husk. *J. Trop. Resour. Sustain. Sci.* **2020,** *8*(2), 94-98. https://doi.org/10.47253/jtrss.v8i2.627.

[43] Hamzezadeh, A.; Rashtbari, Y.; Afshin, S.; Morovati, M.; Vosoughi, M. Application of low-cost material for adsorption of dye from aqueous solution. *Int. J. Environ. Anal. Chem.* **2022,** *102*(1), 254-269. https://doi.org/10.1080/03067319.2020.1720011.

[44] Tan, Y.; Zhang, Z.; Lei, Z.; Yu, L.; Wu, W.; Wang, Z.; Cheng, N. Electronic modulation optimizes OH* intermediate adsorption on Co–Nx–C sites via coupling CoNi alloy in hollow carbon nanopolyhedron toward efficient reversible oxygen electrocatalysis. *Appl. Catal. B* **2022,** *304*, 121006. https://doi.org/10.1016/j.apcatb.2021.121006.

[45] Waliullah, R. M.; Rehan, A. I.; Awual, M. E.; Rasee, A. I.; Sheikh, M. C.; Salman, M. S.; Hossain, M. S.; Hasan, M. M.; Kubra, K. T.; Hasan, M. N.; et al. Optimization of toxic dye removal from contaminated water using chitosan-grafted novel nanocomposite adsorbent. *J. Mol. Liq.* **2023,** *388*, 122763. https://doi.org/10.1016/j.molliq.2023.122763.

[46] Khalfaoui, A.; Bouchareb, E. M.; Derbal, K.; Boukhaloua, S.; Chahbouni, B.; Bouchareb, R. Uptake of methyl red dye from aqueous solution using activated carbons prepared from *Moringa oleifera* shells. *Clean. Chem. Engin.* **2022,** *4*, 100069. https://doi.org/10.1016/j.clce.2022.100069.

[47] Andersen, M.; Reuter, K. Adsorption enthalpies for catalysis modeling through machine-learned descriptors. *Acc. Chem. Res.* **2021,** *54*(12), 2741-2749. https://doi.org/10.1021/acs.accounts.1c00153.

[48] Mendiretta, M. M.; Mudliar, S. L.; Bharati, A. V. Physico-chemical key parameters, Freundlich and Langmuir isotherm, rate constant studies on the removal of divalent nickel using *Delonix regia* fruit pod as low-cost bioadsorbent. *IOP Conf. Ser. Mater. Sci. Eng.* **2022,** *1221*, 012024. https://doi.org/10.1088/1757-899x/1221/1/012024.